Hydrol. Earth Syst. Sci. Discuss., 7, 8703–8740, 2010
www.hydrol-earth-syst-sci-discuss.net/7/8703/2010/
doi:10.5194/hessd-7-8703-2010

Hydrology and Earth System Sciences Discussions

Estimate soil moisture using trapezoidal relationship between remotely sensed land surface temperature and vegetation index

W. Wang, D. Huang, X.-G. Wang, Y.-R. Liu, and F. Zhou

State Key Laboratory of Hydrology-Water Resources and Hydraulic Engineering, Hohai University, Nanjing, 210098, China

Received: 26 October 2010 – Accepted: 26 October 2010 – Published: 3 November 2010

Correspondence to: W. Wang (w.wang@126.com)

Published by Copernicus Publications on behalf of the European Geosciences Union.

Abstract

The trapezoidal relationship between surface temperature (T_s) and vegetation index (VI) was used to estimate soil moisture in the present study. An iterative algorithm is proposed to estimate the vertices of the T_s ~VI trapezoid theoretically for each grid, and then WDI is calculated for each grid using MODIS remotely sensed measurements of surface temperature and enhanced vegetation index (EVI). The capability of using WDI based on T_s ~VI trapezoid to estimate soil moisture is evaluated using soil moisture observations and antecedent precipitation in the Walnut Gulch Experimental Watershed (WGEW) in Arizona, USA. The result shows that, T_s ~VI trapezoid based WDI can well capture temporal variation in surface soil moisture, but the capability of detecting spatial variation is poor for such a semi-arid region as WGEW.

1 Introduction

In 1980s', it was found that, land surface temperature (T_s) and the fraction of vegetation cover, which is represented by vegetation indices (e.g., NDVI), typically show a strong negative relationship (e.g., Goward et al., 1985; Nemani and Running, 1989). Such a relationship has been widely used to investigate the moisture condition of land surfaces. Several studies focused on the slope of the T_s/NDVI curve for providing information on vegetation and moisture conditions at the surface (e.g., Smith and Choudhury, 1991; Nemani et al., 1993). Their approach was later extended to use the information in the T_s/VI scatter-plot space, whose envelope is considered to be in either a triangular shape (e.g, Price, 1990; Carlson et al., 1994), or a trapezoid shape (e.g., Moran et al., 1994).

The idea of triangle T_s/VI space has been used to develop the so called "triangle method", and has been applied by a lot of researchers (e.g., Gillies et al., 1997; Sandholt et al., 2002; Margulis et al., 2005; Tang et al., 2010). The "triangle" method fits the scatter-plot of observed vegetation index (VI) and land surface temperature (T_s) using

HESSD

7, 8703–8740, 2010

a triangle. The central assumption of the triangle method is that, given a large number of pixels reflecting a full range of soil surface wetness and fractional vegetation cover, sharp boundaries (edges) in the data reflect real physical limits: i.e., bare soil, 100% vegetation cover, and lower and upper limits of the surface soil water content, e.g., completely dry or wet (field capacity), respectively. The dry and wet edges ultimately intersect at a (truncated) point at full vegetation cover. Then, based on the triangle, the relative value of surface soil water content and the surface energy fluxes at each pixel can be defined in terms of its position within the triangle. The advantage of the triangle method is its independence of ancillary data. The approach, however, has difficulty in defining the dry and wet edge, especially the dry edge. Even with a large number of remotely sensed observations, the boundaries of the triangle space are still hard to be well established, because on one hand, there are situations when VI–T_s points scatter in a close range such as during rainy season or in areas with a narrow VI range; on the other hand, the T_s~VI relationship is much more complicated at large scale than at local scale and may vary at different parts due to heterogeneity in land surface properties and atmospheric forcing. Furthermore, because the triangle space is established empirically, the soil moisture estimates according to such an empirical triangle using an image at one time are hard to be compared with those at another time.

Moran et al. (1994) proposed the idea of vegetation index/temperature (VIT) trapezoid, and the water deficit index (WDI) for evaluating evapotranspiration rates of both full-cover and partially vegetated sites. However, very few applications were found in the literature based on the idea of trapezoid T_s/VI space for estimating soil moisture. In the present paper, we will extend the idea of VIT trapezoid and WDI, for estimating soil moisture estimation using MODIS products. The method, referred to as the trapezoid method, will be described in detail in Sect. 2. Then the method will be applied to the Walnut Gulch Experimental Watershed in Arizona, USA, for which, the data used and data pre-process will be introduced in Sects. 3 and 4, and the results will be presented in Sect. 5. Finally, some conclusions will be drawn in Sect. 6.

HESSD
7, 8703–8740, 2010

2 Trapezoid method

2.1 The concept of $(T_s - T_a) \sim V_c$ trapezoid

Idso et al. (1981) and Jackson et al. (1981) proposed the CWSI (Crop Water Stress Index) for detecting plant water stress based on the difference between canopy and air temperature. It is designed for full-cover vegetated areas and bare soils at local and regional scales. To overcome the difficulty of measuring foliage temperature in partially vegetated fields, Moran et al. (1994) proposed to use the shape of trapezoid to depict the relationship between the surface temperature and air temperature difference ($T_s - T_a$) vs. the fractional vegetation cover (V_c, ranging from 0 for bare soil to 1 for full-cover vegetation) (Fig. 1), so as to combine spectral vegetation indices with composite surface temperature measurements to allow application of the CWSI theory to partially vegetated fields without a priori knowledge of the percent vegetation cover. Based on the trapezoid assumption and the CWSI theory, Moran et al. (1994) introduced the Water Deficit Index (WDI) for evaluating field evapotranspiration rates and relative field water deficit for both full-cover and partially vegetated sites. For a given pixel with measured surface temperature and air temperature difference, i.e., $(T_s - T_a)_r$, WDI is defined as:

$$\mathrm{WDI} = \frac{(T_s - T_a)_{min} - (T_s - T_a)_r}{(T_s - T_a)_{min} - (T_s - T_a)_{max}} \quad (1)$$

where T_a is air temperature; T_s is surface temperature; the subscripts min, max, and r refer to minimum, maximum, and measured values, respectively; and the minimum and maximum values of $(T_s - T_a)$ are interpolated linearly on the cold edge and warm edge of the $(T_s - T_a) \sim V_c$ trapezoid for the specific V_c value of the pixel. Graphically, WDI is equal to the ratio of distances AC/AB in Fig. 1.

HESSD
7, 8703–8740, 2010

2.2 Calculation of vertices of the $(T_s - T_a) \sim V_c$ trapezoid and its simplification: the $T_s \sim$VI trapezoid

The theoretical basis of $(T_s - T_a) \sim V_c$ trapezoid is the energy balance equation, i.e.,

$$R_n = G + H + \lambda E \quad (2)$$

where, R_n is the net radiant heat flux density ($W\,m^{-2}$), G is the soil heat flux density ($W\,m^{-2}$), H is the sensible heat flux density ($W\,m^{-2}$), and λE is the latent heat flux to the air ($W\,m^{-2}$) and λ the heat of vaporization (kJ/kg).

In their simplest forms, H and λE can be expressed as:

$$H = C_v\,(T_s - T_a)/r_a \quad (3)$$

$$\lambda E = \left[\Delta\,(R_n - G) + C_v\,(\mathrm{VPD})/r_a\right] / \left[\Delta + \gamma\left(1 + r_c/r_a\right)\right] \quad (4)$$

where

- T_s and T_a are the land-surface and air temperature (K), respectively;
- C_v is the volumetric heat capacity of air ($1295.16\,J\,K^{-1}\,m^{-3}$);
- VPD (vapor pressure deficit of the air) (hPa) is calculated as a difference between saturation vapour pressure e_s and actual vapour pressure e_a (hPa), given by (WMO, 2008)

$$e_S = 6.112\exp\left(\frac{17.62\,T_a^{'}}{T_a^{'} + 243.12}\right)\ (T_a^{'} \text{ is the air temperature in °C, } T_a^{'} = T_a - 273.15)$$

$e_a = \mu e_s$, (μ is observed relative humidity)

HESSD
7, 8703–8740, 2010

– Δ is the slope of the curve of saturation water vapour pressure versus air temperature, calculated with (WMO, 2008)

$$\Delta = 4098 \cdot e_s / \left(237.3 + T_a^{'}\right)^2$$

– γ the psychrometric constant (hPa/°C), given by (WMO, 2008)

$$\gamma = 0.646 + 0.0006\, T_a^{'}$$

– r_a the aerodynamic resistance ($s\,m^{-1}$);

– r_c the canopy resistance to vapor transport ($s\,m^{-1}$);

Then, combining Eqs. (2), (3), and (4), we obtain the equation for temperature difference between air and land surface:

$$(T_s - T_a) = \left[r_a (R_n - G)/C_v\right] \left\{\gamma \left(1 + r_c/r_a\right) / \left[\Delta + \gamma \left(1 + r_c/r_a\right)\right]\right\} - \mathrm{VPD}/\left[\Delta + \gamma \left(1 + r_c/r_a\right)\right] \quad (5)$$

As suggested by Moran et al. (1994), for the $(T_s - T_a) \sim V_c$ trapezoid, its four vertices correspond to (1) well-watered full-cover vegetation, (2) water-stressed full-cover vegetation, (3) saturated bare soil, and (4) dry bare soil. Using the energy balance equations, Moran et al. computed the values of the four vertices of the trapezoid as the following:

(1) For full-covered and well-watered vegetation (Point 1)

$$(T_s - T_a)1 = \left[r_a (R_n - G)/C_v\right] \left\{\gamma \left(1 + r_{cm}/r_a\right) / \left[\Delta + \gamma \left(1 + r_{cm}/r_a\right)\right]\right\} - \mathrm{VPD}/\left[\Delta + \gamma \left(1 + r_{cm}/r_a\right)\right] \quad (6)$$

where r_{cm} is the minimum canopy resistance, i.e., canopy resistance at potential evapotranspiration.

HESSD
7, 8703–8740, 2010

(2) For full-covered vegetation with no available water (Point 2)

$$(T_s - T_a)2 = \left[r_a (R_n - G)/C_v\right] \left\{\gamma \left(1 + r_{cx}/r_a\right)/\left[\Delta + \gamma \left(1 + r_{cx}/r_a\right)\right]\right\} - \mathrm{VPD}/\left[\Delta + \gamma \left(1 + r_{cx}/r_a\right)\right] \quad (7)$$

where r_{cx}, is the canopy resistance associated with nearly complete stomatal closure.

(3) For saturated bare soil (Point 3), where canopy resistance (r_c) = 0, we have

$$(T_s - T_a)3 = \left[r_a (R_n - G)/C_v\right] \left[\gamma (\Delta + \gamma)\right] - \mathrm{VPD}/(\Delta + \gamma) \quad (8)$$

(4) For dry bare soil (Point 4), where $r_c = \infty$ (analogous to complete stomatal closure), and $\lambda E = 0$, we have

$$(T_s - T_a)4 = r_a (R_n - G)/C_v \quad (9)$$

The $(T_s - T_a) \sim V_c$ trapezoid considers that relationship between $(T_s - T_a)$ and V_c. Now we think about the issue in another way that, with a given value of T_a, how T_s is related with V_c. To analysis this $T_s \sim V_c$ relationship, we use Eq. (6)~(9) to calculate the T_s for the four extreme cases (or trapezoid vertices) by move T_a in the equations to the right side of the equations. At the same time, V_c is replaced by vegetation index (VI). So that, we modify the structure of the trapezoid, obtaining a simplified $T_s \sim$VI trapezoid with the horizontal axis as VI, and the vertical axis as the surface temperature T_s. We therefore refer the algorithm proposed here to as T_s – VI trapezoid method.

To obtain the values of T_s with Eq. (6)~(9), we need to know r_a, r_c (including r_{cm} and r_{cx}), R_n, G for the four vertices separately, as shown in the following section.

HESSD
7, 8703–8740, 2010

2.3 Calculation of the components in the formula for four vertices of T_s ~VI trapezoid

2.3.1 Aerodynamic resistance (r_a)

The water vapor aerodynamic resistance r_a (s/m) can be estimated with the following equation (Brutsaert, 1982):

$$r_a = \left[\ln\left(\frac{z-d}{z_{0m}}\right) - \psi_m\right]\left[\ln\left(\frac{z-d}{z_{0h}}\right) - \psi_h\right]/k^2\, u_z \quad (10)$$

where

- z is the height (m) above the surface at which u_z and T_a are measured (commonly 2 m);
- u_z is wind speed (m s^{-1}), which could be measured directly;
- d is displacement height (m), given by $d = 0.667h$, and h is the height of vegetation (Garratt, 1992), which should be given as an input.
  z_{0m} is the roughness lengths for momentum (m), given by $Z_{0m} = h/8$ (Garratt, 1992). For bare soil surface, z_{0m} is commonly taken to be 0.01 m (Shuttleworth and Wallace, 1985).
- z_{0h} is the roughness lengths for heat (m), given by

$$z_{0h} = z_{0m}/\exp\left(KB^{-1}\right) \quad (11)$$

Here, KB^{-1} is a dimensionless parameter. Kustas et al. (1989) showed that KB^{-1} is a linear function of the product of u and $T_s - T_a$, given by

$$KB^{-1} = S_{KB} \cdot u \cdot (T_s - T_a) \quad (12)$$

HESSD
7, 8703–8740, 2010

where S_{KB} is an empirical coefficient, which varies somewhere between 0.05 and 0.25.

- k is the von Karman constant ($k = 0.41$);
- ψ_h and ψ_m are the stability corrections for heat and momentum (unitless). ψ_h and ψ_m are calculated differently depend on the atmospheric stability, which could be indicated by the Monin-Obukhov length L, given by

$$L = -\rho\, C_p\, u_*^3\, T_a/(kgH) \tag{13}$$

where $g = 9.8\,\mathrm{m/s^2}$, $k = 0.41$, ρ is the air density ($\mathrm{kg\,m^{-3}}$), C_p the air specific heat at constant pressure ($1004\,\mathrm{J\,kg^{-1}\,K^{-1}}$), $u_* = u_z k/[\ln(z/z_{0m})]$.

For stable situations ($L > 0$),

$$\begin{cases} \psi_m = -5\,(z - z_{0m})/L \\ \psi_h = -5\,(z - z_{0h})/L \end{cases} \tag{14}$$

For unstable conditions ($L \leq 0$),

$$\begin{cases} \psi_m = 2\ln\left(\frac{1+x}{1+x_0}\right) + \ln\left(\frac{1+x^2}{1+x_0^2}\right) - 2\tan^{-1}(x) + 2\tan^{-1} x_0 \\ \psi_h = 2\ln\left(\frac{1+y}{1+y_0}\right) \end{cases} \tag{15}$$

where, $x = \left[1 - 16(z-d)/L\right]^{1/4}$, $x_0 = \left[1 - 16 z_{0m}/L\right]^{1/4}$, $y = \left[1 - 16(z-d)/L\right]^{1/2}$, $y_0 = \left[1 - 16 z_{0h}/L\right]^{1/2}$.

2.3.2 Net radiant heat flux density (R_n)

Net radiation is defined as the difference between the incoming and outgoing radiation fluxes including both long- and shortwave radiation at the surface of Earth. Net radiant heat flux density (R_n) ($\mathrm{W\,m^{-2}}$) can be expressed as:

$$R_n = (1 - \alpha)\, R_s + \varepsilon_a \times \sigma \times T_a^4 - \varepsilon_s\, \sigma\, T_s^4 \tag{16}$$

HESSD
7, 8703–8740, 2010

where

– α is surface shortwave albedo, which can be calculated as a combination of MODIS narrow band spectral reflectance values ($\alpha_1 \sim \alpha_7$) (Liang et al., 1999), given by

$$\alpha = 0.3973\,\alpha_1 + 0.23821\,\alpha_2 + 0.3489\,\alpha_3 + 0.265\,\alpha_4 + 0.1604\,\alpha_5 - 0.0138\,\alpha_6 + 0.0682\,\alpha_7 + 0.0036$$

– R_s is solar radiation, estimated jointly by solar constant, solar inclination angle, geographical location and time of year, atmospheric transmissivity, ground elevation, etc. The basic formula for estimating R_s is (Zillman, 1972):

$$R_s = \frac{S_0 \cos^2 \theta}{1.085 \cos \theta + e_0 (2.7 + \cos \theta) \times 10^{-3} + 0.1}$$

where S_0 is the solar constant at the atmospheric top (1367 w/m^2), θ the solar zenith angle, e_0 is the vapor pressure. In consideration of the effects of topography on the incident short-wave radiation (R_s), the solar zenith angle (θ) is corrected using digital elevation model (DEM) data (Duffie and Beckman, 1991) with the following formula:

$$\cos\theta = \sin(\delta)\sin(\varphi)\cos(s) - \sin(\delta)\cos(\varphi)\sin(s)\cos(r) + \cos(\delta)\cos(\varphi)\cos(s)\cos(\omega) + \cos(\delta)\sin(\varphi)\sin(s)\cos(r)\cos(\omega) + \cos(\delta)\sin(\gamma)\sin(s)\sin(\omega)$$

where ϕ is the latitude (positive in the north hemisphere); s is the slope, and r is the slope orientation, both derived from DEM; δ is solar declination, and ω solar hour angle, given by

$$\delta = 0.409 \sin\left(2\pi \cdot \mathrm{DOY}/365 - 1.39\right)$$

HESSD
7, 8703–8740, 2010

$$\omega = \frac{\pi}{12}(t - 12)$$

where DOY is the day of year, and t is the time when the satellite TERRA pass over the region.

– ε_a is the atmospheric emissivity estimated as a function of vapor pressure, given by Iziomon et al. (2003)

$$\varepsilon_a = 1 - 0.35 \times \exp\left(-10 \times e_a/T_a\right)$$

– ε_s is surface emissivity often evaluated as a function of NDVI. For instance, ε_s could be predicted for the 8–14 µm spectral range from NDVI using $\varepsilon_s = 1.009 + 0.047\,\mathrm{Ln}\,(\mathrm{EVI})$ (Bastiaanssen et al., 1998). Among MODIS Land Surface Temperature and Emissivity products (MOD11), there are emissivity products for band 31 and 32, i.e. ε_{31} and ε_{32}. In the present study, we take the average of the two products to get surface emissivity, namely, $\varepsilon_s = (\varepsilon_{31} + \varepsilon_{32})/2$.

In our algorithm, R_n is not directly solved with the Eq. (16), because T_s is considered as an unknown variable. Instead, we replace the term R_n in Eq. (6)∼(9) with the Eq. (10) respectively, so that we get four quartic equations for T_s at four vertices separately. Then the quartic equations are solved with the iterative algorithm which is shown later in Sect. 2.4 and Fig. 2, by doing so, all the values of T_s for the four vertices are obtained.

2.3.3 Soil heat flux density *G*

G is normally considered to be linearly related to R_n. Several studies have shown that the value of G/R_n typically ranges between 0.4 for bare soil and 0.05 for full vegetation cover (Choudhury et al., 1987). Idso et al. (1975) conducted some experiments investigating the impacts of water content on the net radiation ∼ soil heat flux relationship over bare soil surface, and showed that G/Rn ranges from 0.2 for wet bare soil to 0.5 for dry bare soil.

HESSD
7, 8703–8740, 2010

2.3.4 Canopy resistance (r_c)

Canopy resistance (r_c), including r_{cm} and r_{cx} that refer to the minimum and maxium canopy resistance respectively, should be calculated for Point 1 and Point 2. According to Moran et al. (1994), r_{cm} in Eq. (6) is calculated with r_{sm}/LAI (LAI is the leaf area index, r_{sm} is minimum stomatal resistance). r_{cx} in Eq. (7) is calculated with r_{sx}/LAI (r_{sx} is maximum stomatal resistance).

Values of minimum and maximum stomatal resistance (r_{sm} and r_{sx}, respectively) are published for many agricultural crops under a variety of atmospheric conditions. Moran et al. (1994) suggested that, if values are not available, reasonable values of r_{sm} = 25–100 s/m and r_{sx} = 1000–1500 s/m will not result in appreciable error, we set r_{sm} = 25 and r_{sx} = 1500. Because LAI are mostly less than 8 (Scurlock et al., 2001), we set LAI = 8. Therefore, we have r_{cm} = 3.125 and r_{cx} = 187.5.

2.4 Iterative procedure for calculating T_s

Values of T_s for the four vertices are obtained by an iterative procedure for each pixel. An initial value of r_a is estimated by ignoring the two stability corrections, i.e., ψ_h and ψ_m. With the initial r_a, initial values of T_s are obtained with Eq. (6)~(9) for the four vertices. Then the iterative procedure is proceeded by iteratively changing H, KB^{-1}, r_a, and in consequence, T_s, until the value of T_s is table (i.e., the change of T_s is less than 0.1 k, and the change of r_a is less than 0.1 s/m). Normally, it takes 5 to 10 iterations. While Ts is derived, R_n, G, H, and r_a for each vertex are obtained as well.

The iterative procedure is conducted distributedly based on pixels, that is, the trapezoid is constructed separately for each pixel, and each trapezoid has its own values of T_s.

HESSD
7, 8703–8740, 2010

3 Case study area and data used

3.1 The Walnut Gulch Experimental Watershed

Data of the Walnut Gulch Experimental Watershed (WGEW) was used in the present study. The WGEW is defined as the upper 148 km^2 of the Walnut Gulch drainage basin in an alluvial fan portion of the San Pedro catchment in southeastern Arizona (Fig. 3). It was developed as a research facility by the United States Department of Agriculture (USDA) in the mid-1950s. This rangeland region receives 250–500 mm of precipitation annually, with about two-thirds of it as convective precipitation during a summer monsoon season. The potential evapotranspiration is approximately ten times annual rainfall. The runoff in the ephemeral streams is of short duration and is typically near critical depth. The topography can be described as gently rolling hills incised by steep drainage channels which are more pronounced at the eastern end of the catchment near the Dragoon Mountains. Soil types range from clays and silts to well-cemented boulder conglomerates, with the surface (0–5 cm) soil textures being gravelly and sandy loams containing, on average, 30% rock and little organic matter (Renard et al., 1993). The mixed grass-brush rangeland vegetation ranges from 20 to 60% in coverage. Grasses primarily cover the eastern half of the catchment, while the western half is bush-dominated.

3.2 MODIS data and ground observational data used

The moderate resolution imaging spectroradiometer (MODIS) instrument is very popular for monitoring soil moisture because of its high spectral (36 bands) resolution, moderate spatial (250–1000 m) resolution, and various products for land surface properties. All standard MODIS data products are freely available at NASA Land Processes Distributed Active Archive Center (URL: https://lpdaac.usgs.gov/lpdaac/). MODIS products used in the present study include: MOD09A1 land surface albedo data, MOD11A1 land surface temperature data, and MOD13A1 vegetation data. Details of the products

HESSD
7, 8703–8740, 2010

we used here are listed in Table 1. We selected MODIS data of ten cloud-free days approximately evenly distributed in the period from January to December 2004. All the MODIS data are resampled to 500 m resolution.

Meteorological data required here include air temperature T_a, relative humidity μ, and wind velocity u, observed approximately at the time (11:00 a.m.) when the satellite Terra passes over the WGEW region. The T_a, relative humidity μ, and wind velocity u, are observed at three sites. We take the average of the observations at three sites for μ and u. Observations of T_a are pre-processed, which will be discussed in Sect. 4.3. To evaluate the soil moisture estimation results, soil moisture observations at 16 sites and precipitation data at 87 sites are used. The locations of the 3 meteorological observation sites, 16 soil moisture observation sites and 87 rain gauging sites are plotted in Fig. 4. Because some gauging sites are located on the edge of the watershed, to include the observations at these sites for evaluation, our study area is slightly larger than the WGEW watershed.

In addition, SRTM digital elevation model (DEM) data and land cover data are used.

All the ground data are obtained from the website of United States Department of Agriculture (USDA) Southwest Watershed Research Center (URL: http://www.tucson.ars.ag.gov/dap/).

4 Data pre-processing

4.1 Destriping for MODDIS albedo data (MOD09A1)

MODIS09A1 product includes albedo data of 7 bands. Surface shortwave albedo is calculating as a weighted summation of the albedo data of 7 bands, as shown in Sect. 3.2.2. It was found that the albedo data of the fifth channel has serious problem of bad strips, which would affect the accuracy of surface albedo calculation.

HESSD
7, 8703–8740, 2010

The strips in Band 5 data mostly are lines of one pixel in width, which are distinguishable from neighbouring pixels. To identify the strips, we firstly define the following two convolution kernels:

$$k1 = \begin{bmatrix} 0 & -1 & 0 \\ 0 & 1 & 0 \\ 0 & 0 & 0 \end{bmatrix} \quad k2 = \begin{bmatrix} 0 & 0 & 0 \\ 0 & 1 & 0 \\ 0 & -1 & 0 \end{bmatrix}$$

Then, we calculate $KK = \text{convol}(D, k_1) \times \text{convol}(D, k_2)$, where convol(•) is the convolution filtering function in IDL , and D is the data to be processed. A pixel in a strip is identified if $KK > 0.001$ for this pixel. For bad pixels, linear interpolation is applied to replace the bad values using the values of upside and downside neighboring pixels.

Besides the strips of one pixel width, there are also some strips with two pixels in width resulted from the process of projection conversion in Band 5 of MOD09A1 albedo product. Considering that the pixels in strips have normally higher values than normal, we identify pixels with values larger than 0.35 as "bad" pixels. Then we interpolate the bad pixels with neighbouring "good" pixels with the method of Delaunay triangle (using the program DEM_BAD_DATA_DOIT in IDL). In the same way, pixels with value of 0 are also treated.

With the above two procedures, the quality of Band 5 albedo product was significantly improved (see Fig. 5).

4.2 Denosing the MOD13A1 vegetation index data

When observing the land surface, MODIS is inevitably impacted by the variation of satellite orbital position, cloud coverage and other atmospheric effects. Although several methods (such as Maximum Value Composites or Constrained View Maximum Value Composite) have been applied to reduce the noise impacts the MODIS NDVI/EVI products, quite amount of noise still exist in the VI dataset, and filtering is still necessary when using them for constructing T_s ~VI space.

HESSD
7, 8703–8740, 2010

Many methods are available to denoise the MODIS NDVI/EVI data. Jennifer (2009) compared several methods, and found that the asymmetric Gaussian, Double logistic, and 4253H twice filter perform very well in general. Therefore, one of them, i.e., 4253H twice filter (Velleman, 1980) was adopted here. The 4253H twice filter applies a series of running medians of varying window size and a weighted average filter (e.g., Hanning filter), with re-roughing, to the EVI time series.

To perform the denoising process, a series of continuous EVI data over one year are required. Therefore, before we use the MODIS data selected for 10 dates, we used 25 consecutive 16-day composite EVI data (the last 16-day composite data in 2003, all 23 16-day composite EVI data in 2004, together with the first 16-day composite data in 2005) to conduct the denoising procedure. The effects of denoising for two randomly selected pixels are shown in Fig. 6, from which we see that, both low values and high values are smoothed.

4.3 Topographic correction of air temperature

With methods of estimating soil moisture using thermal satellite images, often both land surface temperature and ground-based air temperature observations are needed. When applying such methods to mountainous regions, terrain effects have to be taken into account because terrain would significantly affect both land surface temperature and air temperature. To avoid the problem of steeply sloping terrain, some authors just eliminated those pixels in mountainous part (e.g., Carlson et al., 1994), while in some other cases, land surface temperature was corrected (e.g., Hassan et al., 2007). In the present study, we go the opposite way, i.e., instead of correct land surface temperature, we correct the air temperature.

To make a successful air temperature interpolation, many factors should be taken into account, such as the difference in elevation between grid points and monitoring stations, temperature vertical gradient, geometric characteristics (slope, aspect) of each grid cell, and vegetation coverage. Moore et al. (1993) proposed a specific algorithm

HESSD
7, 8703–8740, 2010

to calculate daytime temperature at different altitudes within a valley. Based on that, Bellasio et al. (2005) proposed a simplified equation in the form of

$$T_i = T_b - \beta \left(z_p - z_0\right) + C \left(S_i - 1/S_i\right) \left(1 - \mathrm{LAI}_i/\mathrm{LAI}_{max}\right) \quad (17)$$

where T_i is the unknown atmospheric temperature (K) at a z_i altitude (m), T_b is the measured atmospheric temperature (K) at a z_b altitude (m), β is the vertical temperature gradient ($\mathrm{K\,m^{-1}}$), C is a constant, LAI_{max} and LAI_i are, respectively, maximum leaf area index (LAI) and its value at z_i, and S_i is the ratio between direct shortwave radiation on the actual surface (with its slope and aspect) and direct shortwave radiation on a horizontal free surface.

The above equation did not consider the impacts of wind. But according to the research of MccuTchan and Fox (1986), for their study area (an isolated, conical mountain with elevation ranging from 2743 to 3324 m), wind speeds greater than $5\,\mathrm{ms^{-1}}$ negate any slope, elevation or aspect differences present at low wind speed. We approximate this wind effect with a coefficient $e^{-u/3}$ (u is the wind speed), in sequence, obtain a modified equation of Eq. (X) as

$$T_i = T_b - \beta \left(z_i - z_0\right) + C_e^{-u/3} \left(S_i - 1/S_i\right) \left(1 - \mathrm{LAI}_i/\mathrm{LAI}_{max}\right) \quad (18)$$

Therefore, when there are air temperature observations at several sites, we can conduct air temperature correction in the following three steps:

(1) Correct the observations to a flat plane at a base level

All the temperature data are corrected to a flat plane at a base level (the lowest elevation z_0 of the observation sites), considering the effects of not only the elevation difference, but also the effects of wind, slope, and aspect. This is basically a reverse correction of Eq. (X), i.e.,

$$T_{a,b}^{(i)} = T_a^{(i)} + \beta \left(z_i - z_0\right) - C_e^{-u/3} \left(S_i - 1/S_i\right) \left(1 - \mathrm{LAI}_i/\mathrm{LAI}_{max}\right) \quad (19)$$

HESSD
7, 8703–8740, 2010

where $T_{a,b}^{(i)}$ is the temperature observation corrected to the base level at site i, β is the temperature lapse rate (°C/m), z_i is the elevation of site i, and z_0 is the elevation of the base level (m).

(2) Interpolate temperature for each pixel p using observations on the flat plane at the base level

Use the corrected air temperature observations $T_{a,b}^{(i)}$ to interpolate the air temperature for all pixels with a spatial interpolation method (e.g., the inverse distance weighting interpolation method) to get interpolated air temperature $T_{a,l}^{p}$ for each pixel p on the flat plane at the base level.

(3) Topographic correction for each pixel p to its real position using Eq. (18), where T_b is replaced by $T_{a,l}^{p}$. Here we set $LAI_{max} = 10$, $C = 2$ and $\beta = 0.0065$.

5 Application of T_s–VI trapezoid method to WGEW

5.1 Construct T_s–VI trapezoids

Reasonable shape of trapezoid is the essence of all the algorithms based on the T_s-VI relationship for estimating soil moisture. When construct with the algorithm described in Sect. 2, two parameters, i.e., S_{KB} and G/R_n, are set by trial and error process. For the case study area WGEW, we set S_{KB} to be 0.1 for both vegetated points (point 1 and 2) and bare soil points (point 3 and 4), G/R_n to be 0.3 for wet bare soil, 0.4 for dry bare soil, and 0.05 for full vegetation surface.

To show the effectiveness of the calculation for the values of T_s of four vertices, we plot the four vertices of the trapezoids constructed for all the pixels of the WGEW region in four days in four seasons in Fig. 7. All the estimated T_s at each point are plotted in the form of box-and-whisker plot. The data points (solid dots) of T_s vs. EVI are also plotted in the map. From Fig. 7, we see that the constructed trapezoids well characterize the T_s-EVI space, and basically all the T_s-EVI data points are set in the envelope of the trapezoids.

HESSD
7, 8703–8740, 2010

5.2 Calculation of WDI

Based on the constructed T_s-VI trapezoid for each pixel, using the MODIS T_s and EVI data, we calculate the WDI for each pixel p,

$$\mathrm{WDI}^{(p)} = \frac{T_S^{(p)} - T_{S,\,\mathrm{min}}^{(p)}}{T_{S,\,\mathrm{min}}^{(p)} - T_{S,\,\mathrm{max}}^{(p)}} \tag{20}$$

where T_s is surface temperature obtained from MODIS; the subscripts min, max, and r refer to minimum, maximum, and measured values, respectively; and the minimum and maximum values of T_s are interpolated linearly on the dry edge and wet edge of the T_s ~VI trapezoid for the specific VI value of the pixel.

5.3 Comparison with soil moisture observation and precipitation

Using the surface soil moisture observations at 16 sites, we evaluate WDI estimates in several ways: (1) compared separate WDI estimates with ground observations of all 10 dates (Fig. 8); (2) compare the average of WDI estimates with the average ground observations of 10 dates (Fig. 9); (3) compare the WDI estimates with ground observations of each date separately (Table 2).

From the scatter plot of WDI vs. observation in Fig. 8, we see that from the perspective of a whole year, WDI estimates derived with the T_s–VI trapezoid method has a negative correlation (correlation coefficient $R = -0.7232$) with surface soil moisture, which indicates that WDI estimates can be used to detect the temporal variation in soil moisture. Especially on the scale of the watershed, the average WDI is strongly negatively related (correlation coefficient $R = -0.9$) to the average soil moisture observation, as shown in Fig. 9. Although this is not a high correlation, considering that soil moisture in dry environment, such as in semi-arid area, exhibits high spatial variability and potentially rapid rates of temporal change in moisture conditions, the result is reasonably good.

HESSD
7, 8703–8740, 2010

The comparison between the WDI estimates with ground observations of each date (Table 2) shows that, there is basically no correlation between WDI estimates and surface soil moisture observations. This is partly because of the scale effect, i.e., point soil moisture observations are essentially different from grid averaged soil moisture estimates due to sub-grid variability, partly because of the poor capability of using WDI to detect the variation in soil moisture with low spatial variability. Similar phenomena have been observed by some other researchers as well. For instance, Pellenq et al. (2003) noticed that the point-to-point comparison between observations and simulations shows a poor correlation, but a good correlation is obtained when averaging the simulated and observed soil moisture over a length of 100 m. Comparing the distribution of soil moisture observations over the year with that observed instantaneously, we see that the coefficient of variation (CV) for all soil moisture observations at 16 sites in 10 days over a year is 0.771, much larger than the CV for observed soil in each day (ranging from 0.336 to 0.702, with a mean value of 0.528). In consequence, we can use WDI to detect the temporal variation in soil moisture, but it is hard to detect spatial variation in each day, especially for a small watershed with low spatial soil moisture variability.

Despite of the poor performance for characterizing the spatial variability of soil moisture with WDI, by a visual inspection of the WDI maps of the WGEW region of the 10 dates in Fig. 10, we can still see a clear spatial pattern of soil moisture distribution, which indicates that, to some extent, soil moisture variability could be depicted by WDI maps.

We analyzed the impacts of precipitation on soil moisture by calculating the correlation between WDI and antecedent precipitation (AP) of different number of days, and between soil moisture observation and AP of different number of days. The results are illustrated in Fig. 11, which show that WDI and soil moisture observation have similar levels of correlation with AP (one is positive, another is negative), and the maximum correlation occurs when approximately 10-day AP is taken into account. The scatter plot is shown in Fig. 12. The result indicates that, as expected, the temporal variation

HESSD
7, 8703–8740, 2010

of soil moisture (either reflected by ground observations, or by WDI estimates) is significantly dominated by precipitation process.

6 Conclusions

Considerable efforts have been put on using the relationship between soil moisture and index values derived from surface temperature-vegetation index (T_s ~VI) space, which use optical and thermal RS data as input, to estimate soil moisture. In the present study, we simplified the trapezoidal relationship between the surface temperature and air temperature difference ($T_s - T_a$) vs. the fractional vegetation cover, which is proposed by Moran et al. (1994), to a T_s ~VI trapezoid. The trapezoid is constructed separately for each pixel (grid). An iterative algorithm is proposed to estimate the vertices of the T_s ~VI trapezoid theoretically. Then water deficit index (WDI) which is calculated based on the T_s ~VI trapezoid is calculated for each grid using MODIS remotely sensed measurements of surface temperature and enhanced vegetation index (EVI). In the process of construct the T_s ~VI trapezoid, a data pre-processing procedure, including de-striping bad pixels, eliminating the noise contamination in EVI data, and, especially correcting the topographic effects for air temperature data, is conducted.

Using satellite-based MODIS data (land surface temperature data, EVI, etc.), and ground-based on-site soil moisture data and meteorological data (air temperature, relative humidity, and wind velocity) for the Walnut Gulch Experimental Watershed (WGEW) in Arizona, USA, the capability of using WDI to estimate soil moisture is evaluated using (1) a soil moisture observations and (2) antecedent precipitation. The result shows that, T_s ~VI trapezoid based WDI can well capture temporal variation in surface soil moisture, but the capability of detecting spatial variation is poor for such a semi-arid region as WGEW.

Acknowledgements. We are very grateful to USDA Southwest Watershed Research Center for providing observation data of the Walnut Gulch Experimental Watershed. The financial supports from China Postdoctoral Science Foundation (20080431062), the National Science Foundation of China (40771039) and the 111 Project (B08048) are gratefully acknowledged.

HESSD
7, 8703–8740, 2010

References

Bastiaanssen, W. G. M. and Menentia, M.: A remote sensing surface energy balance algorithm for land (SEBAL) 1. Formulation, J. Hydrol., 212, 198–212, 1998.

Bellasio1, R., Maffeis, G., and Scire, J. S.: Algorithms to Account for Topographic Shading Effects and Surface Temperature Dependence on Terrain Elevation in Diagnostic Meteorological Models, Bound.-Lay. Meteorol., 114, 595–614, 2005.

Brutsaert, W.: Evaporation into the Atmosphere: Theory, History and Applications, D. Reidel, Dordrecht, The Netherlands, 299 pp., 1982.

Carlson, T. N., Gillies, R. R., and Perry, E. M.: A method to make use of thermal infrared temperature and NDVI measurements to infer surface soil water content and fractional vegetation cover, Remote Sens. Rev., 9, 161–173, 1994.

Choudhury, B. J., Idso, S. B., and Reginato, J. R.: Analysis of an empirical model for soil heat flux under a growing wheat crop for estimating evaporation by an infrared-temperature based energy balance equation, Agr. Forest Meteorol., 39, 283–297, 1987.

Duffie, J. A. and Beckman, W. A.: Solar engineering of thermal process, 2nd edition, John Wiley and Sons, New York, USA, 1991.

Garratt, J.: The Atmospheric Boundary Layer, Cambridge University Press, New York, USA, 316 pp., 1992.

Gillies, R. R., Carlson, T. N., Cui, J., Kustas, W. P., and Humes, K. S.: A verification of the "triangle" method for obtaining surface soil water content and energy fluxes from remote measurements of the Normalized Difference Vegetation Index (NDVI) and surface radiant temperature, Int. J. Remote Sens.,18, 3145–3166, 1997.

Goward, S. N., Cruickhanks, G. D., and Hope, A. S.: Observed relation between thermal emission and reflected spectral radiance of a complex vegetated landscape, Remote Sens. Environ., 18, 137–146, 1985.

Hassan, Q. K., Bourque, C. P. A., Meng, F. R., and Cox, R. M.: A wetness index using terrain-corrected surface temperature and normalized difference vegetation index derived from standard MODIS products: An evaluation of its use in a humid forest-dominated region of eastern Canada, Sensors, 7, 2028–2048, 2007.

Ian, D. M. , Norton, T. W., and Williams, J. E.: Modelling environmental heterogeneity in forested landscapes, J. Hydrol., 150, 717–747, 1993.

HESSD

7, 8703–8740, 2010

Idso, S. B., Aase, J. K., and Jackson, R. D.: Net radiation – Soil heat flux relations as influenced by soil water content variations, Bound.-Lay. Meteorol., 9, 113–122, 1975.
Idso, S. B., Jackson, R. D., Pinter Jr., P. J., Reginato, R. J., and Hatfield, J. L.: Normalizing the stress-degree-day parameter for environmental variability, Agr. Meteorol., 24, 45–55, 1981.
Iziomon, M. G., Mayer, H., and Matzarakis, A.: Downward atmospheric longwave irradiance under clear and cloudy skies: Measurement and parameterization, J. Atmos. Sol.-Terr. Phy., 65, 1107–1116, 2003.
Jackson, R. D., Idso, S. B., Reginato, R. J., and Pinter, P. J.: Canopy temperature as a crop water stress indicator, Water Resour. Res., 17, 1133–1138, 1981.
Jennifer, N. H. and McDermid, G. J.: Noise reduction of NDVI time series: An empirical comparison of selected techniques, Remote Sens. Environ., 113, 248–258, 2009.
Kustas, W. P., Choudhury, B. J., Moran, M. S., Reginato, R. J., Jackson, R. D., Gay, L. W., and Weaver, H. L.: Determination of sensible heat flux over sparse canopy using thermal infrared data, Agr Forest Meteorol., 44, 197–216, 1989.
Liang, S.: Retrieval of Land Surface Albedo from Satellite Observations: A Simulation Study[J], J. Appl. Meteorol., 38, 712–725, 1999.
Margulis, S. A., Kim, J., and Hogue, T.: A Comparison of the Triangle Retrieval and Variational Data Assimilation Methods for Surface Turbulent Flux Estimation, J. Hydrometeorol., 6, 1063–1072, 2005.
McCutchan, M. H. and Fox, D. G.: Effect of Elevation and Aspect on Wind,Temperature and Humidity, J. Clim. Appl. Meteorol., 25(12), 1996–2013, 1986.
Moran, M. S., Clarke, T. R., Inoue, Y., and Vidal, A.: Estimating crop water deficit using the relation between surface air temperature and spectral vegetation index, Remote Sens. Environ., 49, 246–263, 1994.
Nemani, R. R. and Running, S. W.: Estimation of regional surface resistance to evapotranspiration from NDVI and thermal IR AVHRR data, J. Appl. Meteorol., 28, 276–284, 1989.
Nemani, R. R., Pierce, L., Running, S. W., and Goward, S.: Developing satellite-derived estimates of surface moisture status, J. Appl. Meteorol., 32, 548–557, 1993.
Pellenq, J., Kalma, J., Boulet, G., Saulnier, G. M., Wooldridge, S., Kerr, Y., and Chehbouni, A.: A disaggregation scheme for soil moisture based on topography and soil depth, J. Hydrol. ,276, 112–127, 2003.
Price, J. C.: Using spatial context in satellite data to infer regional scale evapotranspiration [J], IEEE T. Geosci. Remote, 28, 940–948, 1990.

HESSD
7, 8703–8740, 2010

Renard, K. G., Lane, L. J., Simanton, J. R., Emmerich, W. E., Stone, J. J., Weltz, M. A., Goodrich, D. C., and Yakowitz, D. S.: Agricultural impacts in an arid environment: Walnut Gulch case study, Hydrol. Sci. Tech., 9(1–4), 145–190, 1993.

Sandholt, I., Rasmussen, K., and Andersen, J.: A Simple Interpretation of the Surface Temperature/Vegetation Index Space for Assessment of Surface Moisture Status, Remote Sens. Environ., 79(2), 213–224, 2002 .

Scurlock, J. M. O., Asner, G. P., and Gower, S. T.: Global Leaf Area Index Data from Field Measurements, 1932–2000, Data set, available on-line at http://www.daac.ornl.gov from the Oak Ridge National Laboratory Distributed Active Archive Center, last access: 1 August 2010, Oak Ridge, Tennessee, USA, 2001.

Shuttleworth, W. and Wallace, J.: Evaporation from Sparse Crops – An Energy Combination Theory, Q. J. Roy. Meteor. Soc., 111, 839–855, 1985.

Skirvin, S., Kidwell, M., Biedenbender, S., Henley, J. P., King, D., Collins, C. H., Moran, S., and Weltz, M.: Vegetation data, Walnut Gulch Experimental Watershed, Arizona, United States, Water Resour. Res., 44, W05S08, doi:10.1029/2006WR005724, 2008.

Smith, R. C. G. and Choudhury, B. J.: Analysis of normalized difference and surface temperature observations over southeastern Australia, Int. J. Remote Sens., 12(10), 2021–2044, 1991.

Tang, R., Li, Z.-L., and Tang, B.: An application of the T_sVI triangle method with enhanced edges determination for evapotranspiration estimation from MODIS data in arid and semi-arid regions: Implementation and validation, Remote Sens. Environ., 114, 540-551, 2010.

Velleman, P.: Definition and comparison of robust nonlinear data smoothing algorithms, J. Am. Stat. Assoc., 75, 609–615, 1980.

World Meteorological Organization (WMO): Guide to Meteorological Instruments and Methods of Observation, WMO-No. 8 (CIMO Guide), Geneva, 2008.

Zillman, J. W.: A study of some aspects of the radiation and heat budgets of the southern hemisphere oceans, Canberra: Australian Government Publishing Service, Canberra, Australia, 1972.

HESSD

7, 8703–8740, 2010

Table 1. MODIS data used in the present study.

Product ID	Contents	Spatial resolution	Temporal resolution
MO03	Geolocation Data Set	1 km	daily
MOD09A1	Surface Reflectance	500 m	8 days
MOD11A1	Surface Temperature and Emissivity	1 km	daily
MCD12Q1	Land Cover and Vegetation Dynamics	500 m	Yearly
MOD13A1	Vegetation Indices	250 m	8 days
MOD15A2	Leaf Area Index	1 km	8 days

HESSD
7, 8703–8740, 2010

Table 2. Correlation coefficients between WDI estimates with surface soil moisture observations.

DOY	345	290	256	212	168	157	132	75	30	2
R	0.1225	−0.0316	0.0632	0.0775	−0.0447	−0.0775	−0.2049	0.2098	−0.4919	0.0548

HESSD
7, 8703–8740, 2010

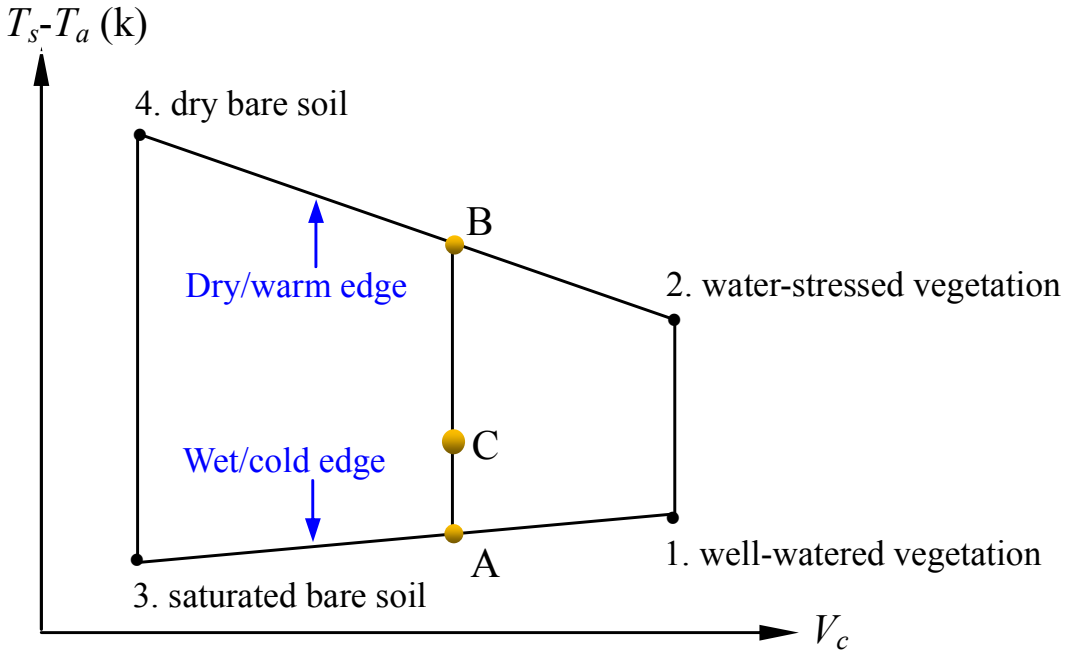

Fig. 1. The hypothetical trapezoidal shape based on the relation between ($T_s - T_a$) and the fractional vegetation cover (V_c).

HESSD
7, 8703–8740, 2010

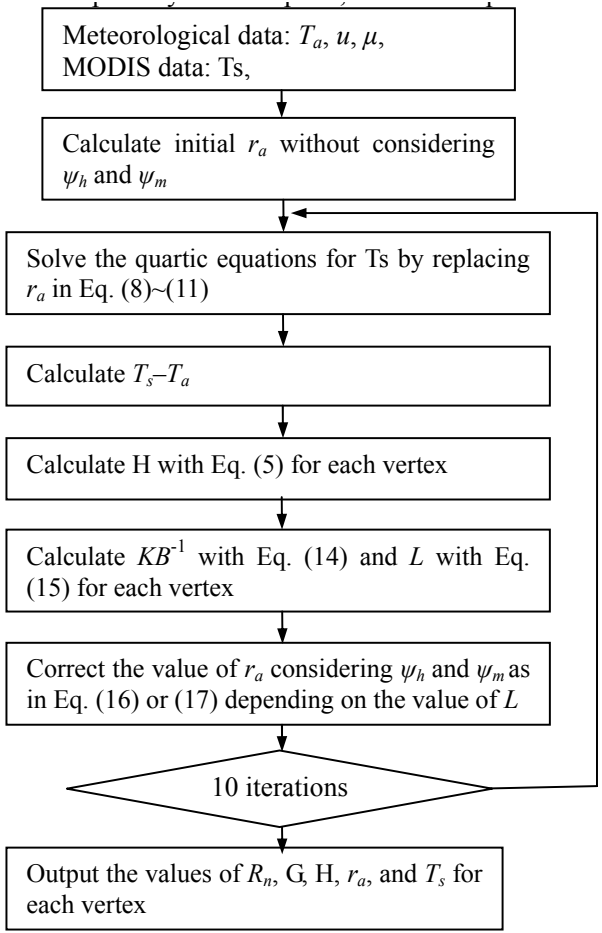

Fig. 2. Iterative procedure for calculating T_s of the four vertices of T_s-VI trapezoid.

HESSD
7, 8703–8740, 2010

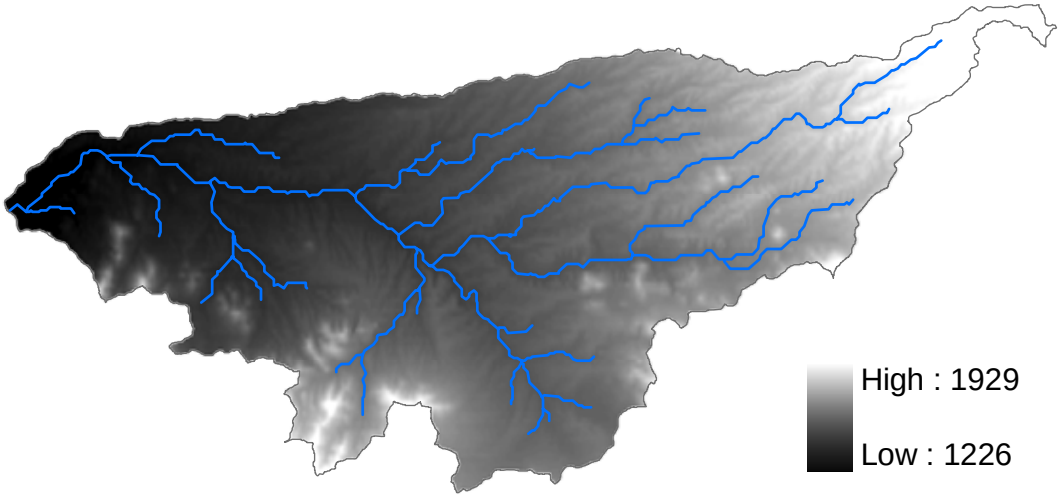

Fig. 3. Digital elevation model (DEM) of Walnut Gulch Experimental.

HESSD
7, 8703–8740, 2010

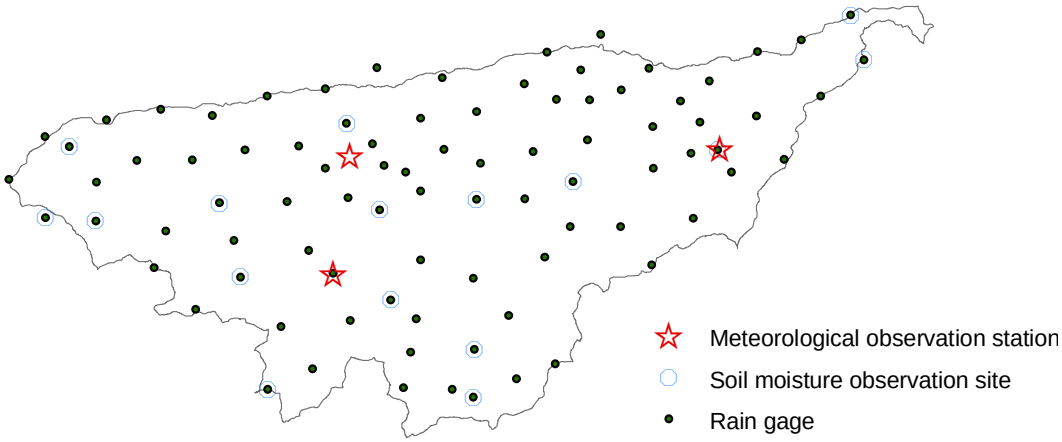

Fig. 4. Locations of ground-based observation sites in WGEW.

HESSD
7, 8703–8740, 2010

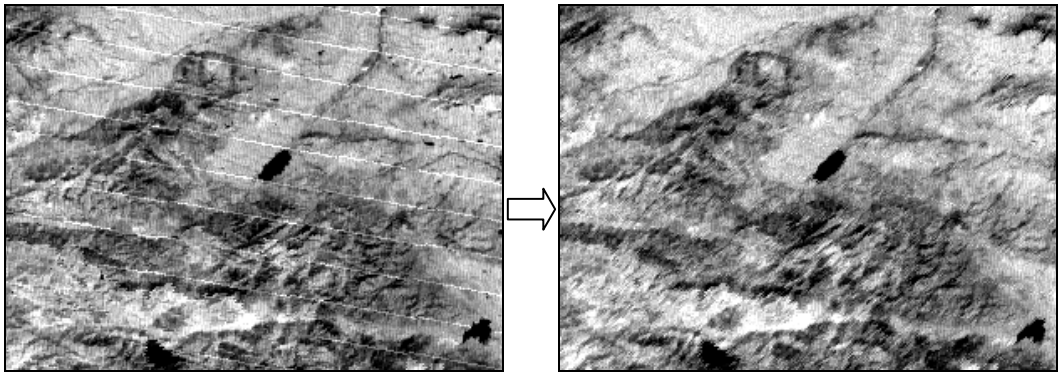

Fig. 5. Comparison of Band 5 albedo images before (left) and after destriping.

HESSD
7, 8703–8740, 2010

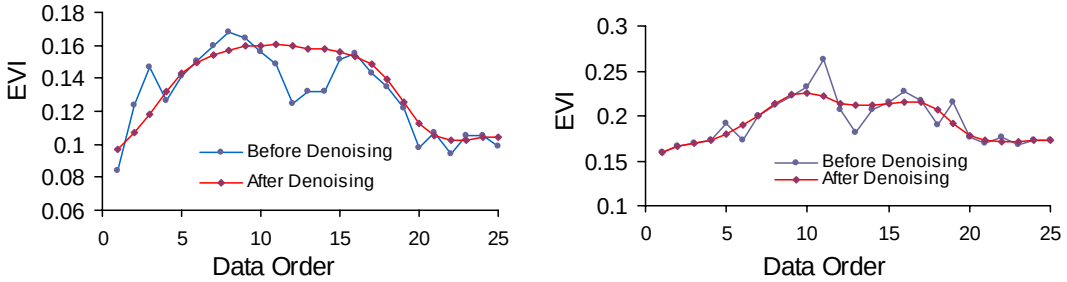

Fig. 6. Effects of EVI denoising preprocessing for two randomly selected pixels.

HESSD
7, 8703–8740, 2010

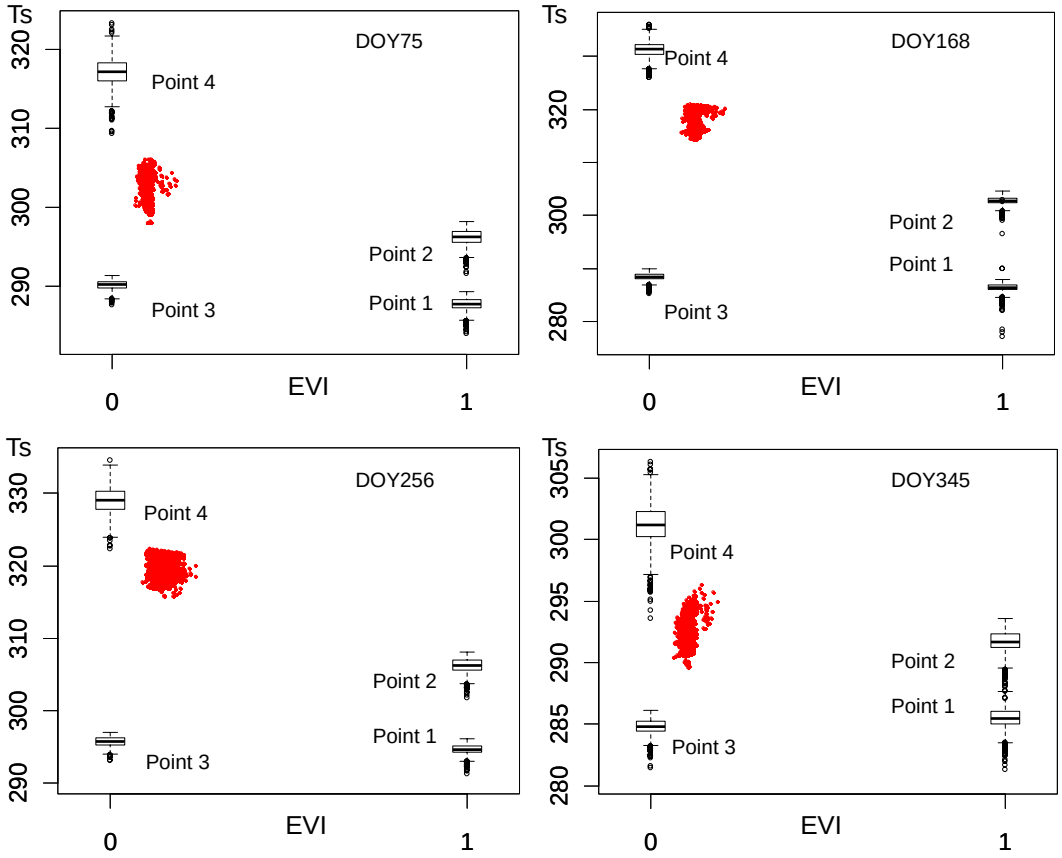

Fig. 7. Constructed T_s–EVI trapezoids in four dates in four different seasons.

HESSD
7, 8703–8740, 2010

Estimate soil moisture using trapezoidal relationship

W. Wang et al.

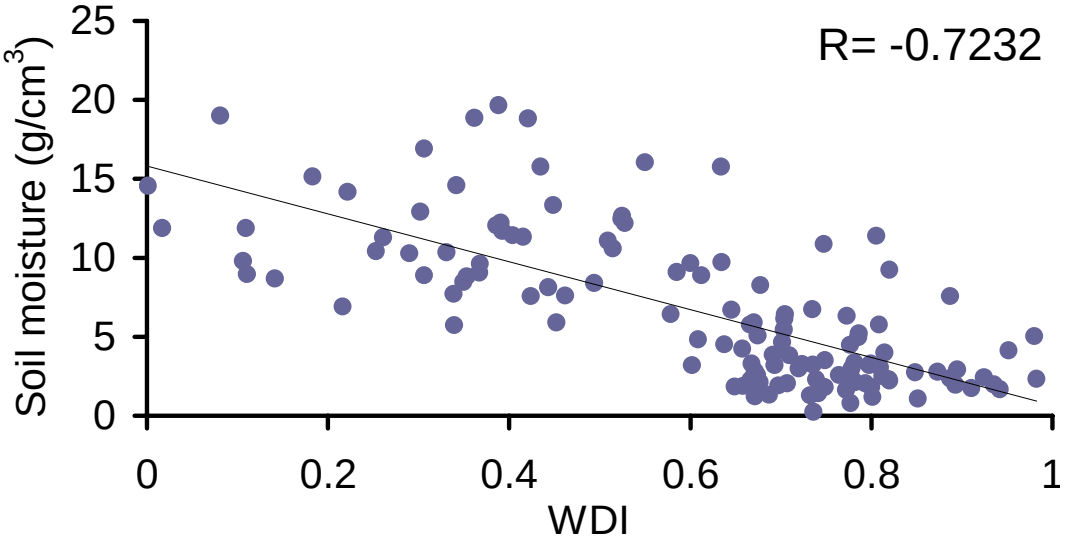

Fig. 8. WDI estimates vs. ground observations at 16 sites in 10 dates (*R* is the correlation coefficient).

HESSD
7, 8703–8740, 2010

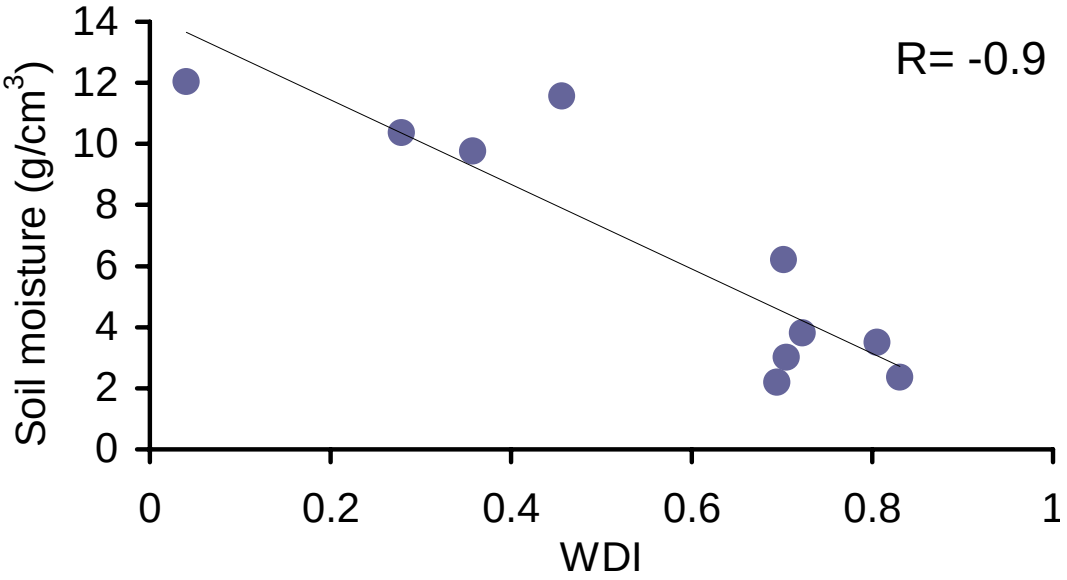

Fig. 9. The average WDI estimates vs. the average ground observations in 10 dates (*R* is the correlation coefficient).

HESSD
7, 8703–8740, 2010

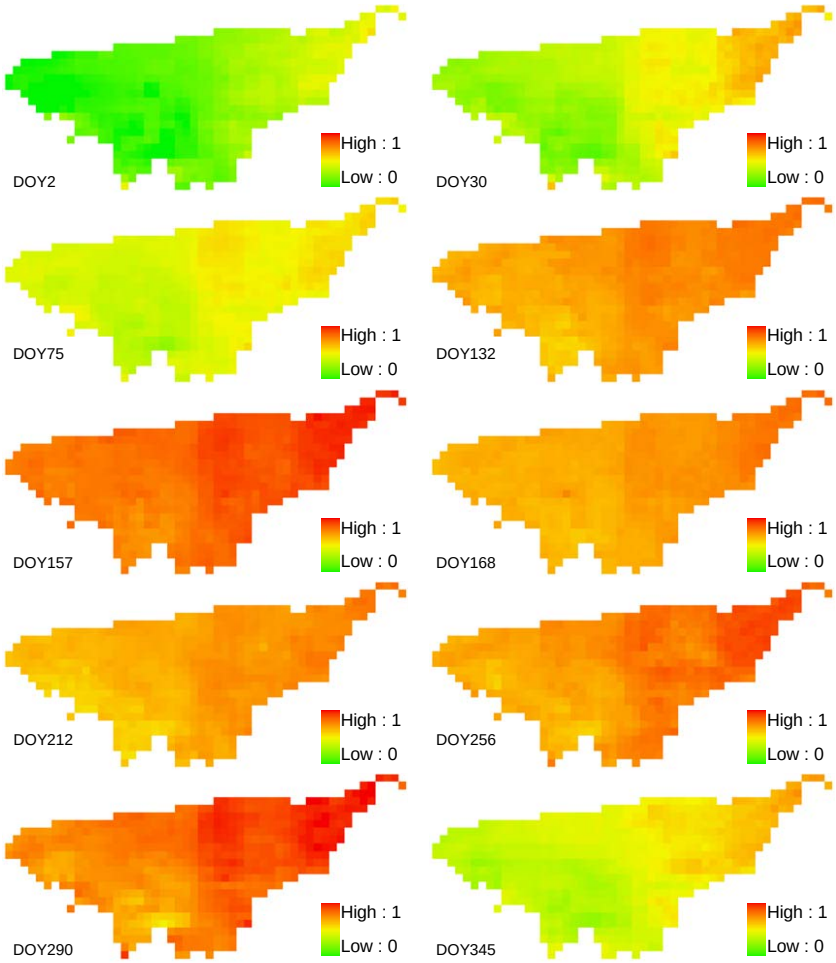

Fig. 10. WDI maps for 10 DOYs.

HESSD
7, 8703–8740, 2010

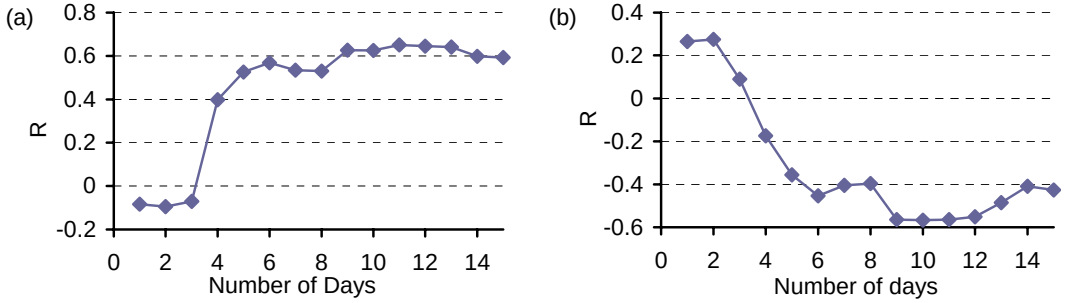

Fig. 11. Correlation coefficient (R) between **(a)** soil moisture observation and AP of different number of days, and **(b)** WDI and AP of different number of days.

HESSD
7, 8703–8740, 2010

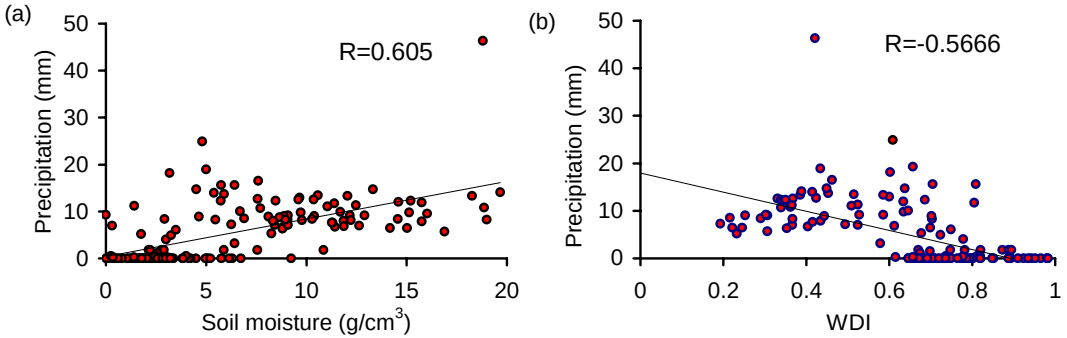

Fig. 12. Scatter plot of **(a)** soil moisture observation and **(b)** WDI vs. 10-day AP (*R* is the coefficient of correlation).

HESSD
7, 8703–8740, 2010